

From Stars to Spheres: A SAXS Analysis of Dilute Dendrimer Solutions

Ty J. Prosa

Department of Physical Sciences, Kutztown University, Kutztown, Pennsylvania 19530

Barry J. Bauer* and Eric J. Amis

National Institute of Standards and Technology, Gaithersburg, Maryland 20899

Received February 4, 2000; Revised Manuscript Received March 15, 2001

ABSTRACT: The progression of intramolecular organizations within a series of dilute poly(amido amine) (PAMAM) dendrimer/methanol solutions is examined by use of small-angle X-ray scattering (SAXS) combined with comparisons to electron density models and radial density distributions extracted by the *indirect transformation for the calculation of $P(r)$* (ITP) method. The SAXS from generation 3 (G3) dendrimers are shown to possess scattering features similar to those of star molecules. This contrasts with the SAXS of the much larger G9 and G10 dendrimers. The G10 SAXS exhibits at least five resolvable secondary maxima. These features are successfully reproduced for a model consisting of constant-density spheres with a small amount of polydispersity in molecular size. Scattering from the intermediately sized G4 through G8 dendrimers reflects a consistent evolution of internal structure progressing from “starlike” to “hard-sphere-like” organizations.

I. Introduction

The ability to precisely control the connectivity and functionality within highly branched polymer systems has expanded avenues for new polymer applications.^{1–7} Because many of these macromolecules possess characteristics reminiscent of biological processes, they may prove useful as fundamental building blocks for designing synthetic materials with desired biological interactions.^{5–7} In addition to the potential applications for highly branched polymers, the ever-expanding litany of newly synthesized dendrimer molecules makes it increasingly important to correlate molecular architecture with the resulting structures and properties.^{8–10}

Dendrimers represent a unique family of precisely engineered, highly branched polymer molecules.¹¹ The number of flavors and types of dendrimers has flourished over the past few years, but the characterization of physical properties has tended to lag behind.^{12–21} In fact, much of the progress in understanding the underlying physics that controls the molecular and bulk properties has come from investigations via computer simulation.^{21–36} These studies have resulted in a variety of expectations about the molecular organization and resulting properties of these materials. Many of these issues have yet to be decided, such as molecular densification as a function of increasing generation, chain backfolding, incomplete generational growth due to overcrowding, and questions of free volume in the interior to allow attachment or capture of agents for drug delivery applications. The detailed understanding of intramolecular and intermolecular organizations within dendrimers remains of critical importance for the evaluation of proposed dendrimer applications, but it also serves to extend our understanding of large, branched polymer systems.

From a purely theoretical perspective, dendrimers are a model system for exploration of the important statistical and physical interactions controlling the microstructure of regularly branched, well-defined, and specifically controlled, “monodisperse” families of polymers. Den-

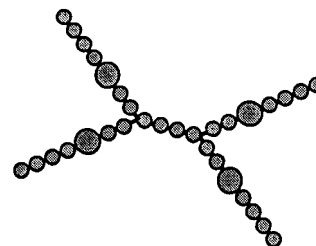


Figure 1. Schematic representation of a four-armed star where beads are used to represent the various linkages present within the core of the PAMAM series of dendrimers.

drimers provide a natural extension to f -functional polymer stars, the simplest branched structures in nature. Polymer stars have been studied as a function of both the number of arms, f , and molecular weight, M_w ,³⁷ of each arm.^{38–41} The variation of these two polymeric parameters provides for a range of properties, from linear chainlike (small f and high M_w arms) to spherelike (high f and low M_w arms). Dendrimers offer investigators the ability to study an additional level of branching complexity in a precisely controlled manner.

Scientists within the dendrimer community often depend on a two-dimensional diagram of chemical bonding to guide their insight into expected organizations and to suggest potential applications (see Figures 1 and 2). At their core, all dendrimers are 3- or 4-armed stars. The M_w of each arm is generally much smaller than that of most reported polymer stars, and unlike traditional polymer stars which vary the number of arms originating at the core, dendrimers exhibit a cascaded branching sequence with additional branch points at the end of each succeeding arm. These additional arms generally have the same M_w as arms within the core, but successive arm attachment is not limited to this simple progression. True convergent dendrimers are “grown” by first completing a generation and then adding additional arms at each available chain end. When a complete “layer” of arms has been added to the dendrimer exterior, another generation is com-

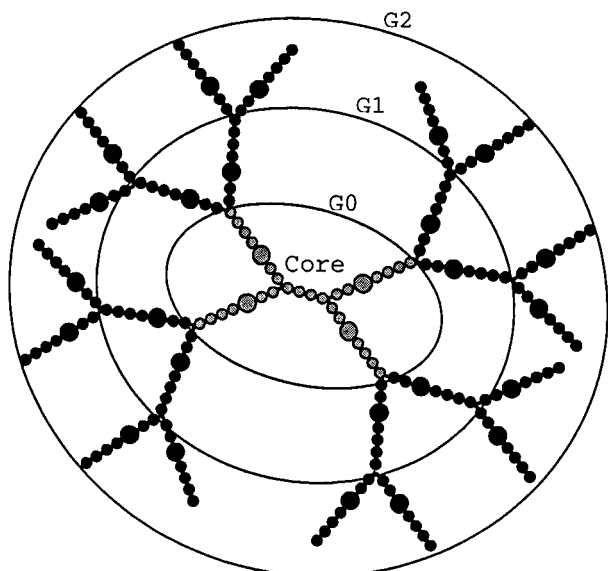


Figure 2. PAMAM G2 dendrimer represented by strings of seven beads and a tetrafunctional core of four beads. Every third bead of the each arm is represented by a bead that has twice the area of the others to approximate the extra scattering cross section of the C–O segment present in these segments. The precursor generations, G0 and G1, are identified to emphasize the controlled nature of dendrimer growth.

pleted. This “protect-de-protect” chemical synthesis ensures a finely controlled molecular architecture. Each new generation or layer of added arms approximately doubles the M_w , the number of arms or spacers, and also the number of branch points. In the limit of large generation to spacer M_w , the amount of volume available for generation growth reaches a theoretical limit.³⁶ Near this theoretical limit the dendrimer molecules have been observed to be spherelike in shape and have a relatively constant internal density profile.¹³ The continued detailed study of these molecules provides a logical step in bridging the gap between the broad understanding of micromolecular structure and more complex polymer systems including gels and highly cross-linked polymers.

The technique of dilute polymer solution scattering to extract structural information about polymer molecules is well developed.^{42–48} These techniques yield indirect information about the molecular organization via comparisons to simulation and known particle scattering functions and direct information by utilization of the *indirect transformation for the calculation of $P(r)$* (ITP) suite of programs. In an earlier study we have shown that the largest generation poly(amino amine) (PAMAM) dendrimers exhibit scattering that comes very close to the scattering expected from a suspension of hard spheres.¹³

This paper reports on the progression of particle scattering for dilute solutions of increasing generation PAMAM dendrimers in methanol. A larger range of scattering angles coupled with improved statistics available from the high flux of a synchrotron light source provides data of sufficient quality to make a more detailed description of the intramolecular organization for this family of dendrimers than previously.¹³ The availability of the ITP method also lends additional credibility to the results and conclusions of the simpler approaches. The scattering trends show a clear progression from starlike to hard-sphere-like scattering. Comparisons are made to various models including the “soft-

sphere” and distributions of spheres and ellipsoids. These comparisons reveal known deficiencies and inadequacies in these particular models and detail some of the known limitations of SAXS techniques applied to dilute polymer solutions; however, this study does provide the most complete picture to date of the intramolecular organizations within these materials.

II. Experimental Section

PAMAM dendrimer/methanol solutions of G3 and G4 dendrimers were purchased from Aldrich Chemical Co., while G5 through G10 PAMAM dendrimer/methanol solutions were obtained from the Michigan Molecular Institute.^{11,49} Each solution was prepared at a concentration of mass fraction 1–5% dendrimer after further dilution with methanol. Each dendrimer consists of a tetrafunctional $\text{[NCH}_2\text{CH}_2\text{N]}$ core and $\text{[-CH}_2\text{CH}_2\text{(C=O)NHCH}_2\text{CH}_2\text{N]}$ spacers and is terminated at the final generation with H_2 .

The SAXS experiments were carried out at the Advanced Polymers Participating Research Team (AP-PRT) beamline X27C (NIST/SUNY Stony Brook/GE/Allied Signal/Montell/Air Force Laboratory) at the National Synchrotron Light Source (NSLS), Brookhaven National Laboratory (BNL).⁵⁰ A double-multilayer (silicon/tungsten) monochromator⁵¹ with a relative energy resolution ($\Delta E/E$) of $\approx 1\%$ was used to obtain photons with a wavelength $\lambda = 1.307 \text{ \AA}$. A three-pinhole collimation configuration⁵² was used to define a beam size of 0.1 mm, and an evacuated scattering path with Kapton⁵³ windows and a sample-to-detector distance of 1–2 m was used. With the scattering vector, q , defined by

$$q = \frac{4\pi \sin \theta}{\lambda} \quad (1)$$

the above experimental configuration results in a maximum measurable scattering range of $0.008\text{--}0.44 \text{ \AA}^{-1}$. Beam monitors both before and after the sample were used to normalize scattering intensities to the incident flux and to correct for transmission through the sample. The reliability of these monitors was somewhat suspect, and resulting intensities cannot be considered as being on an absolute scale. Fuji image plates⁴⁹ were used to collect the two-dimensional (2-d) data with a pixel resolution of 0.2 mm ($\Delta q \approx 0.001 \text{ \AA}^{-1}$). The SAXS solution cells used in this study had thicknesses of 4 mm and were sandwiched between thin mica windows ($\approx 6 \mu\text{m}$). Silver behenate⁵⁴ was used as an angular calibration standard. Background intensities caused by scattering from the windows of the detector vacuum chamber, solution cell, and beam stop overspill were determined by separate measurements and subtracted from the sample data. The 2-d data sets were converted to 1-d, intensity $[I(q)]$ vs q plots with errors estimated using the standard deviation of the mean for values within the circular annulus defined by the specific annular q value and given by the function

$$\sigma(q) = \sqrt{\frac{n \sum I(q)^2 - (\sum I(q))^2}{n^2(n-1)}} \quad (2)$$

where n is the number of pixels within the 2-d circular annulus and the sum is over all the pixels within the annulus. Data collection times ranged from 1 to 6 h for each scattering curve presented in this paper.

III. SAXS Results and Discussion

Scattering curves obtained from polymer solutions, after corrections for instrumental and solvent scattering effects, consist of contributions from molecular size and shape (intramolecular correlations) and intermolecular correlations. The scattering from a group of monodis-

perse, globular particles can be expressed generally in terms of

$$I(q) = kNP(q) S(q) \quad (3)$$

$$P(q) = I(q)/kNS(q) \quad (4)$$

where q is the scattering vector defined in eq 1, $I(q)$ is the experimental scattering intensity, k is an electron density contrast factor, N is the number of particles, $P(q)$ is the single particle scattering function, and $S(q)$ is the interparticle scattering function accounting for interference effects between particles. A working definition for "dilute" solution is a solution where the approximation $S(q) \approx 1$ holds over the entire observable q range. For "semidilute" solutions, $S(q)$ has a form that slightly depresses $I(q)$ at very low- q scattering angles but behaves as $S(q) \approx 1$ for a majority of the observable q range. The advantage of a semidilute solution experiment over a more concentrated one is that interparticle interactions which affect changes in the particle scattering function are unlikely to exist, so $P(q)$ is identical for both dilute and semidilute solutions. Consequently, the quality of the high- q scattering data is improved for subsequent modeling comparisons with an N -fold increase in desired scattering intensity.

For the data reported in this paper, mass fraction 1% solutions can be considered to be in the "dilute" regime (no low- q downturn), while mass fraction 5% solutions exhibit a small downturn at low- q with no significant interference effect discernible for $q > 0.05 \text{ \AA}^{-1}$. The high- q scattering regions of the mass fraction 5%, semidilute solutions have 5 times the signal-to-background ratio when compared to the mass fraction 1%, dilute solutions. For $q > 0.15 \text{ \AA}^{-1}$ the SAXS background components (methanol, scattering cell, and instrument) constitute 90% or more of the scattering signal. In particular, the Kapton film used as an entrance window for the scattering beam path projects a broad peak near $q = 0.35 \text{ \AA}^{-1}$ that makes it nearly impossible to acquire data of acceptable quality for $q > 0.30 \text{ \AA}^{-1}$. The availability of semidilute scattering data in this report provides sufficient scattering power in this region to overcome background effects and extends the usable q range to just greater than 0.40 \AA^{-1} in some cases. The extension of the useful q range is of critical importance when trying to ascertain the existence of scattering structure at high q or when trying to adequately determine power-law behavior for measured scattering curves.

The general scattering features for three general types of polymer molecular structures (linear chains, stars, and spheres) are shown in Figure 3. The three curves were derived from analytical expressions for a linear chain, a 16-armed polymer star, and a constant-density sphere.⁴⁵ The chain and the star scattering functions were derived assuming Gaussian correlation statistics for each of the monomers within the chain and no excluded volume effects. Under many circumstances, these assumptions are justified, but not in the case of dendrimers. Since dendrimers do not fit the definition of any typical polymer type, yet possess some of the general bonding characteristics of each, it is useful to compare the general scattering trends. For example, linear chains exhibit scattering that is relatively featureless, while polymer stars exhibit a peak when viewed as a modified Kratky plot [$I(q) * q^{5/3}$ vs q]. This

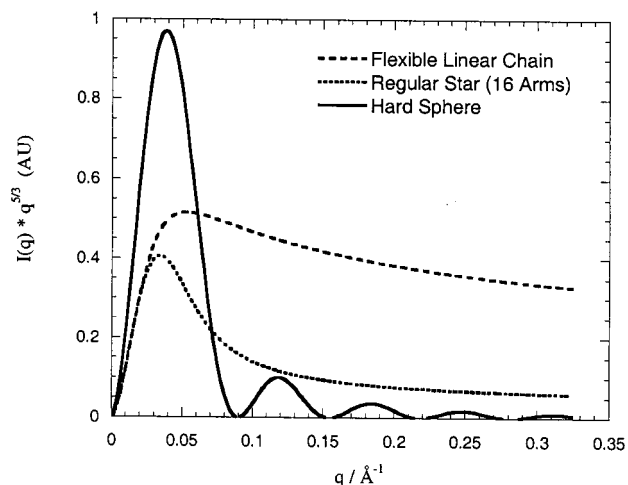


Figure 3. Comparisons of scattering trends for three different molecular organizations: a flexible, linear chain (dashed line), a regular star (dotted line), and a "hard" sphere (solid line).

difference is generally attributed to the more compact nature of the more conformationally limited star.

The scattering from a constant-density sphere is quite different from either a simple chain or a star. The modified Kratky plot of a sphere has a central peak as well as a number of distinctive secondary extrema. These secondary features are due to a combination of an abrupt truncation of the particle electron density and a minimum amount of particle symmetry or, in other words, the sharp transition between the interior of the particle and the exterior solvent and a nearly spherical symmetry.

To generalize better the varying degree of hard-particle and soft-chain character present within the dendrimer, it is not only important to note the presence of scattering structure, but it is also important to note the limiting power-law behavior of these scattering curves. Polymer stars are known to exhibit a q^{-2} power-law behavior in the high- q limit when excluded-volume effects are not significant and a $q^{-5/3}$ power-law behavior when the self-avoiding random walk is considered⁴¹ while particles with sharp interfaces between particle and solvent exhibit q^{-4} power-law behavior.⁵⁵ For scattering entities that can be described as a geometrical particle, the sharpness of the interface between particle and solvent can be cause for a greater than q^{-4} power-law behavior. An important experimental limitation in extracting limiting power-law behavior from experimental curves is the fact that a SAXS experiment measures a fixed " q -window". Depending on the dendrimer's overall size, this q -window may capture part or none of the limiting power-law region.

The experimental SAXS curves obtained from dilute dendrimer/methanol solutions are shown in Figure 4 as a log-log plot in arbitrary intensity units and scaled to best display their distinctive features. Because of the scattering variation present in most of the scattering curves, power-law exponents were determined via graphical methods displayed in the figure. Reported uncertainties of the measured values were estimated by varying the levels of background subtracted from the raw scattering curves within limits determined for each data set. The power-law scattering behavior is observed to evolve from $q^{-5/3}$ for G3 and G4 dendrimers (top) to q^{-4} for G10 (bottom) while the number of secondary maxima increase from zero for G3 to five for G10. Values

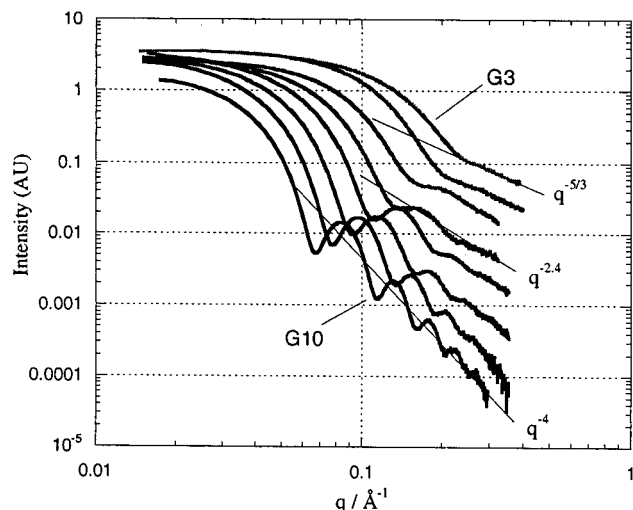


Figure 4. SAXS curves for PAMAM mass fraction 1% dendrimer/methanol solutions of generation G3 (top) through G10 (bottom). The progression of secondary features and limiting power-law behavior suggest an evolving intramolecular organization. The uncertainties are not plotted because they cannot be distinguished from the data line in a plot of this type. See Figure 5 for the uncertainties of these data.

for the measured power-law scattering are listed in Table 1.

The dendrimer sizes were extracted from the SAXS data curves by weighted nonlinear least-squares fits to two types of scattering models: a polydisperse system of spheres (eq 5) and a monodisperse system of ellipsoids of revolution (eq 6).

$$P_{\text{spheres}}(q) = \int_0^{\infty} P_{\text{sphere}}(q,r) \omega(r,w,R) dr \quad (5a)$$

$$P_{\text{sphere}}(q,r) = \frac{9\pi}{2(qR)^3} J_{3/2}^2(qr) \quad (5b)$$

$$\omega(r,w,R) = \frac{\sqrt{\ln 2}}{w\sqrt{\pi}} \exp\left(-\ln 2 \frac{(r-R)^2}{w^2}\right) \quad (5c)$$

$$P_{\text{ellipsoid}}(q) = \int_b^a P_{\text{sphere}}(q,r) \omega(r) dr \quad (6a)$$

$$\omega(r) = \frac{r}{\sqrt{(r^2 - a^2)(b^2 - a^2)}}; \quad a = \text{major axis}, \\ b = \text{minor axis} \quad (6b)$$

$$I(q) = AP(q) + B \quad (7)$$

In these equations $J_{3/2}(qr)$ is a $3/2$ -order Bessel function, R is the mean radius of the distribution of spheres, and w is the half-width at half-maximum of the Gaussian distribution function, $\omega(r,w,R)$, which describes the polydispersity in sphere radii. An arbitrary scaling factor, A , and an arbitrary background, B , described in eq 7, were used so that there were four free parameters in the fitting process (A , B , R , w). B is used to account for imperfections in corrections to the raw SAXS data (primarily error in subtraction of the solvent). Because each data point is weighted by the counting statistics, the points with the smallest q values have a strong influence on the choice of the best fit parameters, especially when these data do not exhibit a q^{-4} power law. Therefore, even though some of these curves do not have the appropriate power-law behavior, they can be

fit by a sphere function. Rather than choose a particular q range for each fit, all available data were used, and the algorithm was allowed to effectively “choose” the range. Fits to truncated q ranges were also performed, but only small changes were observed in the final extracted parameters. Standard Guinier fits to data sets to determine the radius of gyration, R_g , were not used in this work (for more discussion on this point, see ref 13); however, R_g values were calculated from the various fits and displayed in Table 1.

The scattering form function for an ellipsoid of revolution, $P_{\text{ellipsoid}}(q)$, is equivalent to a particular distribution of spheres, $\omega(r)$, where a and b describe the major and minor axes of the ellipsoid of revolution and r takes on all values between a and b .^{56,57} Again, an arbitrary scaling factor, A , and an arbitrary background, B , described in eq 7, were used so that there were four free parameters in the fitting process (A , B , a , b).

To first order, the scattering curves from the various dendrimer solutions are very similar to each other with the primary differences being accounted for by variations in particle size due to M_w . All the scattering curves in Figure 4 have a peak centered at $q = 0$. The width of this peak is inversely related to the overall size of the molecule in solution. The G3 sample has the broadest $q = 0$ peak followed by G4 through G9 while the G10 sample has the most narrow peak. This relationship can be more clearly distinguished in Figure 5 where each of the scattering curves have been scaled by R_g . Dendrimers of generation greater than G4 have a first relative minimum at a qR_g value near 3.65, which corresponds to the position one would expect a minimum if the particles were constant density or “hard” spheres. Scattering from the larger G6 dendrimer solutions appear to have a distinguishable second minimum with the number and quality of succeeding extrema progressively increasing for G7 through G9 solutions. The G10 solution has the most clearly distinguishable extrema including easily identifiable second-, third-, fourth-, and fifth-order minima. These additional higher-order features are highly suggestive of a more compact scattering object like that of the sphere and resemble those scattering features shown in Figure 3, resulting primarily from an abrupt truncation of the particle density and a “ringing” effect observed in the Fourier transform.

It is important to note that there is some experimental uncertainty with regard to the exact limiting power law for the curves reported in this work. These uncertainties are primarily due to three factors. First, the transmission coefficient values needed for proper subtraction of background components were only certain to relative values of $\pm 20\%$. This is based on previous experience at X27C as well as the presence of a peak from the Kapton background scattering that provides a fingerprint identifying incorrect background subtraction. Second, a very weak particle scattering signal at high q , coupled with the previously mentioned instrumental peak in the background profile due to Kapton windows at the beam path entrance, contributed to poor statistics in this region. Third, the presence of a significant but finite q range that may not have extended adequately into the limiting power-law regime for the smallest dendrimers.

The trends in the power-law scattering behavior for these dendrimers support a related progression in particle structure. The scattering from the G3 and G4 dendrimers resembles that of a polymer star in both its

Table 1. Dendrimer Sizes^a

generation	distribution of spheres			ellipsoid of revolution			limiting power law
	R (Å)	w (% R hwhm)	R_g (Å)	A (Å)	C/A	R_g (Å)	
G3	18.8 ± 0.1	18.4 ± 0.5	14.7	21.7 ± 0.1	0.518 ± 0.006	14.7	-1.7
G4	23.0 ± 0.1	17.6 ± 0.5	18.0	26.3 ± 0.1	0.539 ± 0.003	17.8	-1.7
G5	28.2 ± 0.1	10.3 ± 1.8	21.9	31.2 ± 0.1	0.693 ± 0.011	22.0	-1.8
G6	36.3 ± 0.1	14.1 ± 0.4	28.3	40.7 ± 0.1	0.623 ± 0.006	28.1	-2.0
G7	41.9 ± 0.3	10.0 ± 0.9	32.5	45.5 ± 0.4	0.738 ± 0.013	32.4	-2.4
G8	50.2 ± 0.1	9.1 ± 0.2	38.9	54.1 ± 0.2	0.754 ± 0.006	38.7	-2.7
G9	59.2 ± 0.1	7.8 ± 0.2	45.9	63.1 ± 0.1	0.784 ± 0.003	45.6	-3.5
G10	69.9 ± 0.1	7.0 ± 0.1	54.1	74.1 ± 0.1	0.810 ± 0.003	53.9	-4.0

^a Values for the average radius, R , of a Gaussian distribution of spheres is compared to that of a single ellipsoid of revolution. Equivalent radius of gyration values, R_g , for each measurement as well as limiting power-law exponents are also listed. Included error estimates reflect a 95% confidence level of parameters based on the weighted nonlinear least-squares fit; however, other well-known experimental uncertainties limit the overall precision of these measurements to $\pm 5\%$. Power-law exponents are known to ± 0.3 .

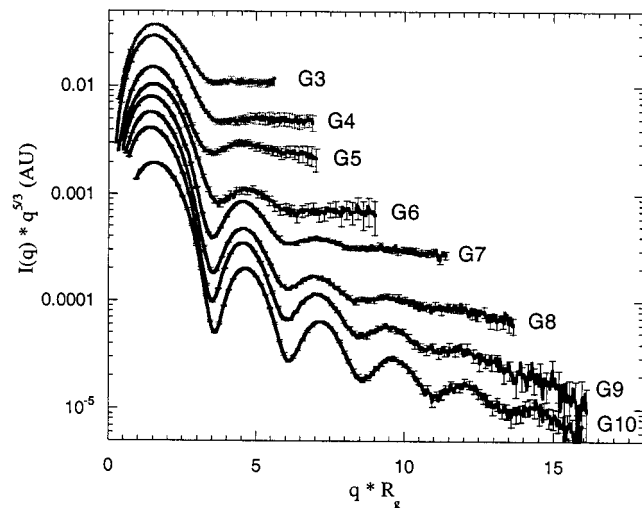


Figure 5. SAXS curves in Figure 4 (G3 top, G10 bottom) have been scaled by their measured radius of gyration (as listed in Table 1) and multiplied by $q^{5/3}$. The self-similarity of the curves and the progression of limiting power-law behavior can be easily identified.

shape and $q^{-5/3}$ power-law dependence. It is difficult to distinguish between a $q^{-5/3}$ and q^{-2} power law because of the uncertainties noted above, but these data are most consistent with a starlike structure where excluded-volume effects are significant. At the other extreme, the scattering from the G10 dendrimer resembles that of a sphere in both its shape and q^{-4} power-law dependence and is indicative of a 3-dimensional geometrical particle with a sharp interface. For intermediate dendrimer generations (G5 to G9), the limiting power-law behavior progresses from greater than $q^{-5/3}$ to less than q^{-4} , suggesting a consistent evolution from starlike to sphere-like scattering. Because the scattering behavior does not fit conveniently into star or sphere scattering, it is difficult to make direct comparisons to well-known particle scattering factors. There are however a number of mean-field and Monte Carlo computer simulations that have reported scattering factors for dendrimers.^{21–35} A qualitative comparison with these simulations can be made. At the size-scale extremes, where the dendrimers more closely resemble stars or spheres, comparisons to analytical scattering form factors can also be made.

For this paper, we have chosen to make “quantitative” comparisons to models that best reflect both the expected and measured segment-density profiles. For G3 dendrimers, the Flory–Stockmayer theory allows for the derivation of a scattering particle function that describes the scattering for a dendrimer bonding configuration

that ignores excluded-volume effects. These calculations do not take into account all molecular interactions, but they do provide some insight into the general scattering behavior for these molecules. The intermediate generation dendrimers do not suggest comparisons with any particular analytically derived particle scattering function, but a comparison to other types of models or simulations reported in the literature can be made. It is apparent that for dendrimers of higher M_w , with greater numbers of arms or branch points, specifically G9 and G10 dendrimers, the scattering profiles lose most of their chainlike characteristics and scatter more like solid bodies. These scattering curves can be fit quantitatively to solutions of hard spheres or other geometrically solid bodies that have little or no polydispersity in size and shape. The result is a measure of the distribution of particle sizes present in these high-generation dendrimers and a convolution of various size–shape characteristics that limit our ability to specifically account for the contribution of each separate characteristic.

IV. Modeling and Discussion

A. PAMAM Dendrimers G3 and G4 as Soft Spheres. The scattering from the G3 dendrimer qualitatively resembles that of a polymer star and is very similar to the curve shown in Figure 3. The particle scattering curves for linear polymers, stars, and branched structures including dendrimers have been calculated using the Flory–Stockmayer and cascade theories.^{45,58}

$$N^2 P(q) = \sum_{j=1}^N \sum_{k=j}^N \phi_{jk}; \quad \phi_{jk} = \phi^{|j-k|} \approx e^{-b^2 q^2/6} \quad (8)$$

The “soft-sphere” model is the term given to the particle scattering factor calculated in this manner for dendrimers and detailed in eq 8. Here N is the number of atom sites within the molecule, b is the bond length between atom sites, and the double sum is over contributions from all possible atom pairs including the self-scattering term ($j = k$). This calculation assumes perfectly flexible Gaussian chains and makes no consideration for excluded-volume effects. In effect, this model approximates the dendrimer architecture as a web of “beads” where the bond length, b , is fixed and the neighboring bead positions are averaged over all possible configurations.

The soft-sphere model calculation was performed for segment bonding arrangements corresponding exactly to those in Figures 1 and 2. This model includes a core of four beads with branching chain segments that

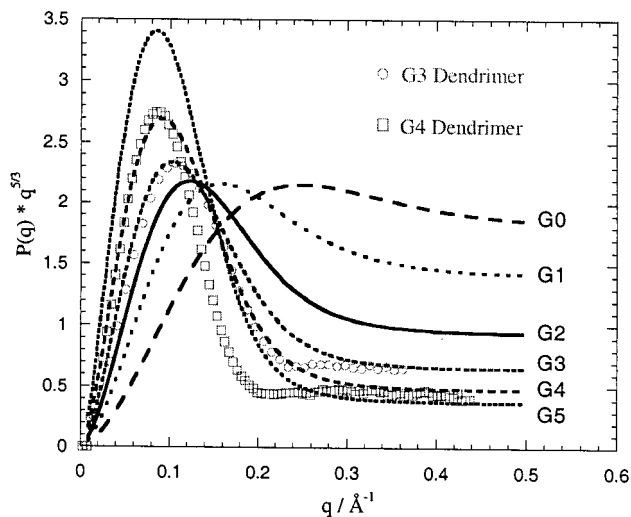


Figure 6. G3 (circles) and G4 (squares) PAMAM dendrimer SAXS are compared to scattering from a theoretical “soft-sphere”, G0 (top) through G5 (bottom). This model shows a progression of central peak width, height, and peak height/tail ratio as a function of generation. A model bond length of 4.0 Å was chosen to match the peak position of the G3 soft-sphere model with the G3 PAMAM data.

consist of seven beads each. The third bead in each chain is weighted twice that of its neighbors in order to approximate the additional scattering power of the C=O bead compared to the CH₂ and NH beads. The only adjustable parameters in this model are the particular bonding configuration, which is predetermined for the PAMAM dendrimers, and the bond length between the beads.

The soft-sphere model results in calculated scattering curves that are very similar to polymer stars and are shown in Figure 6 from G0 (top) through G5 (bottom). As dendrimer generation is increased, this model predicts a narrowing of the Kratky peak and a high- q scattering progression that evolves toward a $q^{-5/3}$ power-law behavior. The fact that this model ignores excluded-volume effects partially explains the absence of structure at high q as well as the $q^{-5/3}$ power-law behavior.

Scattering from G4 dendrimers (see Figures 4 and 5) begins to show weak signs of scattering structure at high q , suggesting that excluded-volume effects begin to have an influence on structure for generations greater than G3. A lack of high- q structure is proposed to be a scattering signature for the crossover from starlike molecular structure to a more compact spherical structure where excluded-volume effects become more important in dendrimer molecules. The ability to discern whether these scattering differences manifest themselves into measurable mechanical or physical traits has yet to be established.

When compared directly to the G3 (circles) and G4 (squares) particle scattering curves in Figure 6, the soft-sphere model is not able to fit the data very well. A bond length of 4.0 Å was chosen to best match the overall position of the model peak in the Kratky plot with that of the data. The overall disagreement between the model scattering prediction and the experimental results suggests that excluded-volume effects and non-Gaussian chain statistics combine to play a role in these highly branched structures, even for the smaller generation dendrimers.

B. PAMAM Dendrimers G9 and G10 as Polydisperse Hard Spheres. For the largest available den-

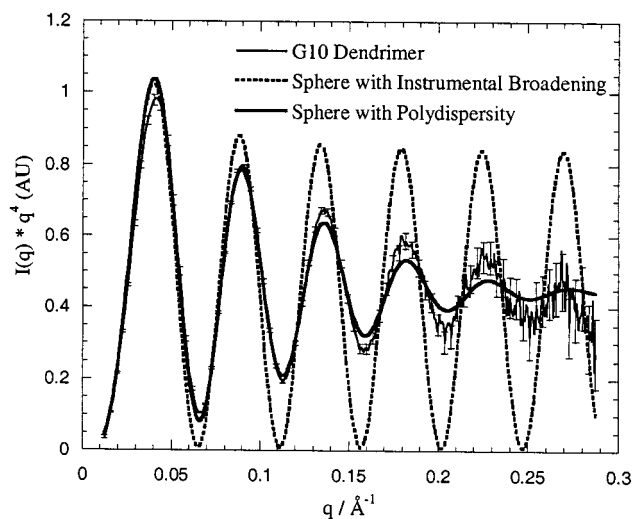


Figure 7. Comparative effects of instrumental broadening (dotted line) and polydispersity (thick solid line) applied to the scattering function of a sphere. When scaled as an $I(q)q^4$ plot, the instrumental broadening causes each higher-order feature to be broadened equally while the polydispersity causes an enveloping effect. The PAMAM G10 data are plotted for comparison.

dendrimer generations, model scattering calculations were performed using of analytical expressions generally available in the literature or by defining a radial electron density distribution, $\rho(r)$, and calculating the particle scattering factors. Particle scattering factors for spherically symmetric objects can be obtained by integrating over contributions made from infinitesimally thin shells of electron density.^{42–45}

$$P_{\rho}(q) = \left(\int_0^{\infty} \rho(r) \left(\frac{\sin qr}{qr} \right) 4\pi r^2 dr \right)^2 \quad (9)$$

Likewise, particle scattering factors for geometrical entities such as spheres and ellipsoids can be found in the literature⁵⁹ or calculated by using eq 9. Particle scattering factors for constant density spheres and ellipsoids are listed in eqs 5 and 6, respectively. Equation 6 has been cast in a form that emphasizes its equivalence to a particular polydisperse distribution of scattering spheres, $\omega(r)$, which represents the fraction of spheres with a particular radius r . Consequently, when only scattering information is available, a dilute solution of ellipsoids cannot be distinguished from that of a slightly polydisperse solution of spheres. All fits to experimental curves were carried out using a weighted nonlinear least-squares algorithm.

It is important to note the possible misinterpretation of instrument broadening effects with elliptical particle shape and polydispersity in particle dimensions. Figure 7 demonstrates how the contributions due to experimental broadening influence the scattering from a particle shaped like a sphere. Here the particle scattering factor for a single sphere (eq 5b) has been convolved with a Gaussian instrumental broadening function that closely matches the characteristics of those observed at the AP-PRT beamline (dotted line). This instrumentally broadened curve can be compared to that of a dilute solution of spheres with a small amount of polydispersity in size or as a single elliptically shaped particle calculated from eq 6. The higher-order features of the single sphere, plotted as a $I(q)q^4$ vs q plot, maintain an equal amount of smearing as a function of

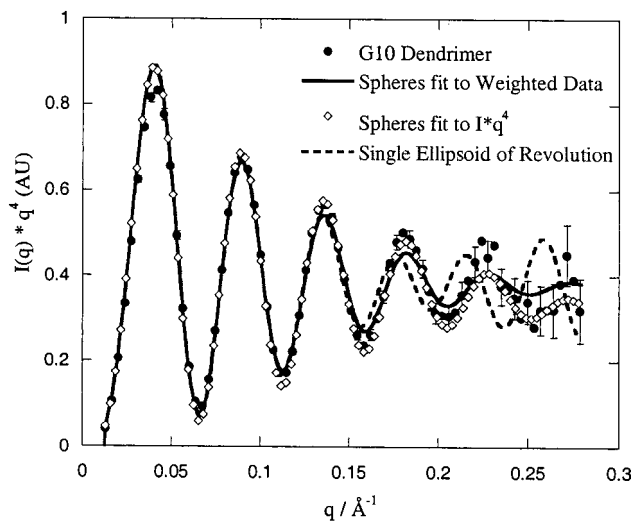


Figure 8. Fits of the G10 PAMAM dendrimer data to a distribution of spheres and a single ellipsoid of revolution (dashed line). The $I(q)q^4$ plot overemphasizes the differences between the fit and the data but better displays the distinctive features of the data at high q . Fits to data equally weighted by $I(q)q^4$ (dotted line) as well as weighted to the uncertainties (thick solid line) are displayed for comparison.

q , whereas the polydisperse curve (thick solid line) exhibits an envelope effect where the secondary extrema approach an average value with a progressive decrease in the peak to valley height as a function of increasing scattering angle. In this particular example, the narrow instrumental broadening function allows one to easily distinguish between these competing effects, thus ruling out instrumental broadening as the primary contributor to structure observed in the scattering for the larger PAMAM dendrimers.

In performing this fitting exercise, we were primarily interested in learning about the sensitivity of the various models to three issues: polydispersity in molecular size, variations in molecular shape, and the possible presence of a “hole” or depression in segment density at the interior of the molecule. Figure 8 shows the results of fits to the G10 SAXS with a distribution of constant-density spheres and a single ellipsoid of revolution. To illustrate the differences between apparent quality of fits, the distribution of spheres model was fit to G10 SAXS data using data points weighted as $I(q)q^4$ with data points weighted by their uncertainties (error bars are included in the figure).

Because the particle scattering curve for an ellipsoid is equivalent to a distribution of spheres, broadening of the extrema due to particle size and shape becomes intermingled. For illustration purposes, the distribution of spheres relevant for the fits displayed in Figure 8 for a single ellipsoid and a distribution of spheres is displayed in Figure 9.

The best-fit parameters for a Gaussian distribution of spheres were $R = 69.9 \pm 4.9 \text{ \AA}$ and $R = 69.8 \pm 4.2 \text{ \AA}$ (where the uncertainty values are half-width at half-height) for data-weighted errors and $I(q)q^4$, respectively (average radius, $R \pm \text{hwhm}$ of a Gaussian distribution). The best-fit ellipsoid of revolution had a major axis, $a = 74.1 \text{ \AA}$, and minor axis, $c = 59.8 \text{ \AA}$ (also see Table 1). These two models fit the data equally well. Realistically, some contributions from both the size and shape variations exist in real PAMAM dendrimers, and a model that has both these variations present may improve the quality of the fit yet would not reveal any new informa-

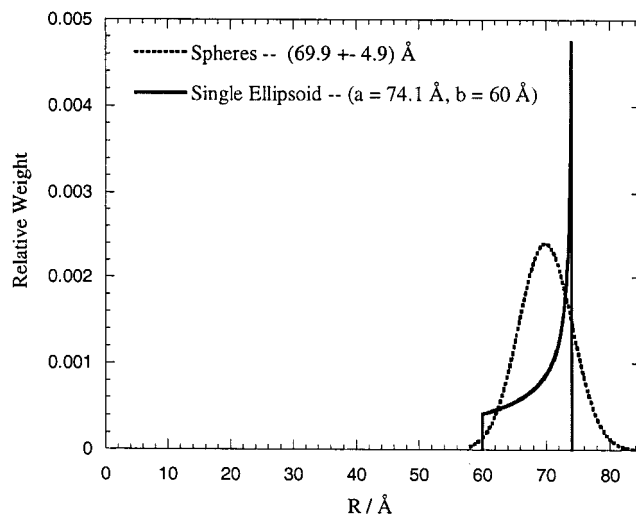


Figure 9. Equivalence of the ellipsoid of revolution from Figure 8 to a distribution of scattering spheres (solid line). The distribution of spheres weighted by the uncertainties used in Figure 8 is also plotted for comparison (dotted line).

tion. The apparent significant differences at high q are overemphasized by the $I(q)q^4$ plot as suggested by the two distribution-of-sphere fits. The best-fit ellipsoid model puts a limit on the amount of particle shape variation present in these dendrimers, and the polydisperse sphere model puts a limit on the amount of size polydispersity present.

At one extreme, it can be assumed that variations in M_n account for any variations in molecular size. (The fractional solvent capacity is assumed to be independent of size for this narrow range.) The polydispersity index, f , for a distribution of molecular sizes $\omega(r)$ has the following relationship:

$$f = \frac{\overline{M_w}}{\overline{M_n}} = \frac{\int r^6 \omega(r) dr}{\left(\int r^3 \omega(r) dr \right)^2} \quad (10)$$

On the basis of the fits to the PAMAM G10 dendrimer data with a polydisperse distribution of spheres, we find $f = 1.032$. Because of the reasons stated above, this number represents a maximum polydispersity index assuming molecules that are exactly spherical in shape. This measured polydispersity index is consistent with those determined by other methods including electron microscopy,⁶⁰ electrospray, and predictions based on defects leading to polydispersity.⁶¹ It is also interesting to note that when one compares the average measured ellipticity for G10 dendrimer from electron microscopy by measuring an average major and minor axis dimension, the result is an ellipsoid with average dimensions similar to that obtained in this study by fitting the G10 scattering with a single elliptically shaped scatterer.⁶²

Finally, it is of considerable interest to determine whether a “hole” or depression in segment density within the interior of the dendrimer is available to facilitate placement of guest species. It has been demonstrated experimentally that this type of guest/host relationship is possible;⁶³ however, the presence of molecular polydispersity (even though small) and a limited available q range (due to physical constraints and from counting statistics) limit the ability to resolve this effect in the SAXS profiles. After attempting various simulations of models with holes, we were unable to

identify significant changes in modeled scattering profiles for holes smaller than 5–10 Å with a relative 10–20% depression in segment density. Only when these depressions are identical from molecule to molecule would one expect to be able to observe the resulting modifications to the observed scattering intensity. The “polydispersity” in hole size and shape necessarily smears out these effects which are convolved with the dominant effects of the overall particle polydispersity in size and shape.

C. PAMAM Dendrimers G5 through G8. Since these PAMAM generations G5 through G8 exhibit scattering that is less than ideal (not readily identifiable as starlike or spherelike), they do not lend themselves to the curve-fitting exercises carried out in the previous sections. However, these materials do exhibit clear evidence of an evolution from starlike to spherelike particle character based on the variations in scattering structure and power-law behavior. For this particular set of dendrimers, it is likely that the excluded-volume effects ignored in the soft-sphere model begin to influence observed scattering and eventually dominate the segment density distribution resulting in roughly spherical compositions for the largest dendrimers.

Various computer simulations of dendrimer structure have resulted in a general disagreement about predicted dendrimer segment distributions.^{21–36} These simulations predict equilibrium structures ranging from a compact, center concentrated^{21–26,34} to a more Gaussian profile of radial segment density^{27,31} to less dense structures.³⁶ Many of these studies report segment density distributions that do not agree with the results observed here, but in order for an adequate comparison to be made between simulation and SAXS experiment, simulation structure factors must be calculated and reported. In addition, there is need for further simulation to a high generation number so that the presence of spherelike scattering structure might be observed.

In particular, the work by Mansfield^{23–25} agrees with some of the general scattering trends reported in this paper. These simulations might be considered an extension of the soft-sphere model where excluded-volume effects are taken into account in a simplified way. Dendrimer molecules were built on a diamond lattice and allowed to relax into an equilibrium state. The loss of conformational freedom imposed on the molecule by the lattice is equivalent to giving the molecular segments some stiffness. No two segments are allowed to occupy the same site, providing for the inclusion of excluded volume in the simulation. Particle scattering factors were calculated, and the general trends match our experimental observations, at least for the smaller molecules. Larger dendrimers are more difficult to simulate because of added computational time, but Mansfield’s G6 through G9 dendrimers do exhibit scattering structure at high- q consistent with the data reported here. However, the experimentally observed variation in power-law behavior is not demonstrated.

D. Pair Correlation Functions and Radial Density Distributions. The corrected scattering curves, $I(q)$, were Fourier transformed into their pair distance distribution functions, $P_C(r)$, and radial distribution functions, $\rho(r)$, using the ITP suite of programs developed by Glatter.^{46–48} This process allows smoothing of the primary data by a weighted least-squares procedure, estimation of the optimum stabilization parameter based on a stability plot, and transformation into real

space by the ITP method. Details of this type of calculation appear elsewhere.^{46–48}

Transform methods have been used in our laboratories to model PAMAM dendrimers that contain gold nanoclusters.⁶⁴ While the dendrimers themselves appeared spherelike, the ones containing nanoclusters revealed a structure of gold clusters being enclosed within the dendrimer and with the clusters being offset from the center of the dendrimer. The ability to resolve the gold nanocluster within the dendrimer was dependent on the fact that the gold particles could be described by a completely uniform interior with a sharp interface. The calculation was additionally aided by the fact that there was sufficient X-ray contrast between the solvent/PAMAM/gold regions to fit this layered model well.

The model that we have used in this study is the same as the one above but without the enclosed nanoclusters. The pair correlation function, $P_C(r)$, is related to the particle scattering factor, $P(q)$, through an integral relationship:

$$P(q) = 4\pi \int_0^\infty \frac{P_C(r) \sin(qr)}{qr} dr \quad (11)$$

To convert from the pair correlation function to the radial distribution function, $\rho(r)$, an integral transformation can be used as

$$P_C(r) = r^2 \int_{-\infty}^\infty \rho(r) \rho(x-r) dx \quad (12)$$

General transform methods require scattering data from $q = 0$ to infinity, so with finite q range data extrapolations are necessary at both high and low q . The ITP method is able to minimize the effects of missing data, and further it requires that a certain number of low- q data points be excluded in order to minimize the effects of interparticle scattering. Since the goal of our present work was to examine the high- q power-laws, higher dendrimer concentrations were used to “magnify” the weak scattering intensities in this q range. This means that several low- q points were necessarily eliminated before application of the ITP method to minimize these effects on the resulting real-space functions. As part of this transform procedure, two other parameters were specified: the maximum possible particle radius and a Lagrange multiplier for required data smoothing. Although the choice of maximum particle radius was somewhat subjective, its choice was observed to affect the calculated distributions only slightly.

The pair correlation functions were calculated using the ITP method for dendrimers from G3 through G10. Figure 10 shows the results of these transformations. The presence of increasing correlation lengths with generation is consistent with the increasing sizes of the dendrimers as listed in Table 1. The similarity in the shapes of the distributions is evident with only slight differences in distribution shape appearing at the larger values of radius, which are the points that are the most sensitive to data from low- q scattering regions.

The radial distribution function shapes are more obviously affected by the generation number. Figure 11 shows the radial distribution functions, and they reveal increasing dendrimers size with generation. G10 shows the sharpest interface between dendrimer interior and exterior with a very slight minimum in segment density at the center and a maximum extension of about 45 Å. The density “drop-off” becomes more gradual as the

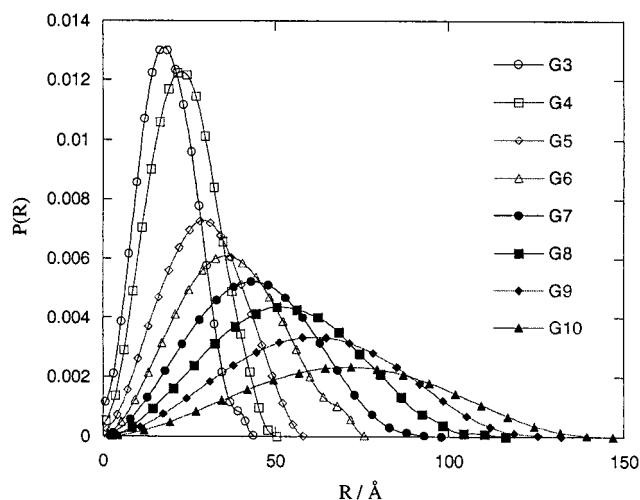


Figure 10. Pair distance distribution functions for G3 through G10 extracted via the ITP method. The evolution of particle size is evidenced by the breadth of the distance distribution function.

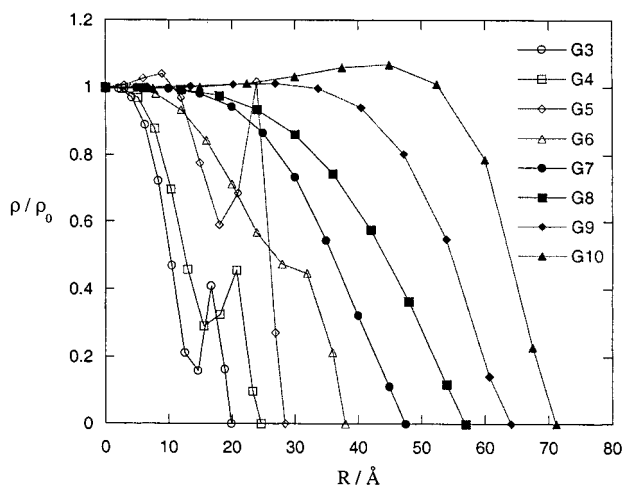


Figure 11. Radial electron density distribution functions, $\rho(r)$, for G3 through G10 extracted via the ITP method. Dendrimers are shown to become larger with sharper particle interfaces as a function of increasing dendrimer generation.

generation number decreases until G7, beyond which the interface regions behave somewhat erratically. This erratic behavior may be a consequence of dendrimers with more starlike power laws not fulfilling the assumption that the scattering particles have spherical symmetry and axial uniformity. Figure 10 shows that the correlation functions follow a smooth progression from G7 through G10.

It is important to note that the calculations performed in this section are for monodisperse distributions of objects. We have demonstrated earlier in this paper that some polydispersity surely exists in these dendrimer solutions, and some or all of the variation of the shapes of the scattering curves may be explained by a polydispersity of geometric sizes and shapes. Accommodation for this fact would result in modifications in the shape of the ITP extracted transition zones of the dendrimers.

V. Conclusions

The overall evolution of the dendrimer internal structure is not surprising. G0 PAMAM dendrimers are, by definition, 4-armed star polymers, and through G3 or G4, these materials exhibit scattering that is very

starlike or qualitatively consistent with the scattering expectations of Flory–Stockmayer and reported experimental scattering for stars. Nevertheless, the cascade procedure proves inadequate for quantitative analysis. Excluded-volume effects already play a role for G3 dendrimers, causing a quantitative disagreement between the soft-sphere model and observed scattering data.

As the dendrimer generation progresses from G5 to G8, higher-order features indicative of a more compact structure occur, and power-law behavior progresses from greater than q^{-2} to less than q^{-4} . These features may be a product of excluded-volume effects. Finally, as the PAMAM dendrimer generation reaches G9 and G10, the scattering features are consistent with a slightly polydisperse collection of hard spheres. This result does not necessitate that the largest dendrimer structures assume perfectly spherical shapes with a constant internal density, but it does indicate fairly narrow limits on the amount of variation in size, shape, and local internal density.

The dendrimer growth process results in a molecular configuration that evolves toward that of a perfect “hard” sphere. It is likely that defects resulting from the imperfect and incomplete chemical synthesis couple to enhance this molecular structure. Defects are not allowed to propagate or are allowed to propagate in such a way that the molecule takes on the spherical structure. This progression is reflected in the polydisperse sphere fits to the experimental data. The distribution widths in Table 1 narrow significantly up to the point where the limiting power-law behavior approaches that of a geometrical body.

Are there other important effects in addition to the random bead walk with excluded volume? The answer is almost certainly yes. The chemical compatibility of the chain ends is usually different from that of the interior segments so one would expect some entropic exclusion of chain ends to the molecular surface. Future scattering characterization with labeled terminal segments in a range of dendrimer generations would surely provide additional insight into these interesting macromolecules.

Acknowledgment. The authors are grateful to a number of people for their contributions to this work. We are thankful to Professor Donald Tomalia and co-workers for making available a range of dendrimer materials and to Professor Benjamin Hsiao and Dr. Fengji Yeh for their assistance in data acquisition at the AP-PRT beamline. The authors are especially grateful to Dr. John Barnes for his particular insights and stringent commitment to the promotion and implementation of quality SAXS techniques. This work was funded in part by the U.S. Army Research Office under Contract 35109-CH.

References and Notes

- (1) Tabakovic, I.; Miller, L. L.; Duan, R. G.; Tully, D. C.; Tomalia, D. A. *Chem. Mater.* **1997**, *9*, 736.
- (2) Margerum, L. D.; Campion, B. K.; Koo, M.; Shargill, N.; Lai, J.-J.; Marumoto, A.; Sontum, P. C. *J. Alloys Compd.* **1997**, *249*, 185.
- (3) Jansen, J. F. G. A.; Peerlings, H. W. I.; de Brabander-Van den Berg, E. M. M.; Meijer, E. W. *Angew. Chem., Int. Ed. Engl.* **1995**, *34*, 1206.
- (4) Jiang, D.-L.; Aida, T. *Nature* **1997**, *388*, 454.
- (5) Astruc, D. *C. R. Acad. Sci. II B* **1996**, *322*, 757.
- (6) Urich, K. *Trends Polym. Sci.* **1997**, *5*, 388.

- (7) Rizzuto, C. D.; Wyatt, R.; Hernandez-Ramos, N.; Sun, Y.; Kwong, P. D.; Hendrickson, W. A.; Sodroski, J. *Science* **1998**, *280*, 1949.
- (8) Labarre, J.-F.; Sournies, F.; Crasnier, F.; Labarre, M.-C.; Vidal, C.; Faucher, J.-P.; Graffeuil, M. *Phosphorus, Sulfur, Silicon* **1996**, *109–110*, 525.
- (9) Gorman, C. B.; Parkhurst, B. L.; Su, W. Y.; Chen, K.-Y. *J. Am. Chem. Soc.* **1997**, *119*, 1141.
- (10) Galliot, C.; Larre, C.; Caminade, A.-M.; Majoral, J.-P. *Science* **1997**, *277*, 1981.
- (11) Tomalia, D. A.; Naylor, A. M.; Goddard, W. A. *Angew. Chem., Int. Ed. Engl.* **1990**, *29*, 138.
- (12) Tomalia, D. A.; Baker, H.; Dewald, J.; Hall, M.; Kallos, G.; Martin, S.; Roeck, J.; Ryder, J.; Smith, P. *Polym. J.* **1985**, *17*, 117.
- (13) Prosa, T. J.; Bauer, B. J.; Amis, E. J.; Tomalia, D. A.; Scherrenberg, R. *J. Polym. Sci., Part B: Polym. Phys.* **1997**, *35*, 2913.
- (14) Jackson, C. L.; Chanzy, H. D.; Booy, F. P.; Drake, B.; Tomalia, D. A.; Bauer, B. J.; Amis, E. J. *ACS PMSE Proc.* **1997**, *77*, 222.
- (15) Topp, A.; Bauer, B. J.; Amis, E. J.; Scherrenberg, R. *ACS PMSE Proc.* **1997**, *77*, 82.
- (16) Hummelen, J. C.; vanDongen, J. L. J.; Meijer, E. W. *Chem. Eur. J.* **1997**, *3*, 1489.
- (17) Kleppinger, R.; Reynaers, H.; Desmedt, K.; Forier, B.; Dehaen, W.; Koch, M. *Macromol. Rapid Commun.* **1998**, *19*, 111.
- (18) Kleppinger, R.; Reynaers, H.; Desmedt, K.; Forier, B.; Dehaen, W.; Koch, M.; Verhaert, P. *Macromol. Rapid Commun.* **1998**, *19*, 111.
- (19) Prosa, T. J.; Bauer, B. J.; Topp, A.; Amis, E. J.; Scherrenberg, R. *ACS PMSE Proc.* **1998**, *79*, 307.
- (20) Bauer, B. J.; Topp, A.; Prosa, T. J.; Liu, D.; Jackson, C. J.; Amis, E. J. *SPE ANTEC* **1998**, *98*, 2065.
- (21) Scherrenberg, R.; Coussens, B.; van Vliet, P.; Edouard, G.; Brackman, J.; de Brabander, E.; Mortensen, K. *Macromolecules* **1998**, *31*, 456.
- (22) Murat, M.; Grest, G. S. *Macromolecules* **1996**, *29*, 1278.
- (23) Mansfield, M. L. *Polymer* **1994**, *35*, 1827.
- (24) Mansfield, M. L.; Klushin, L. I. *Macromolecules* **1993**, *26*, 4262.
- (25) Mansfield, M. L.; Klushin, L. I. *J. Phys. Chem.* **1992**, *96*, 3994.
- (26) Lue, L.; Prausnitz, J. M. *Macromolecules* **1997**, *30*, 6650.
- (27) Lescanec, R. L.; Muthukumar, M. *Macromolecules* **1990**, *23*, 2280.
- (28) Lach, C.; Brizzolara, D.; Frey, H. *Macromol. Theory Simul.* **1997**, *6*, 371.
- (29) La Ferla, R. *J. Chem. Phys.* **1997**, *106*, 688.
- (30) Cai, C.; Chen, Z. Y. *Macromolecules* **1997**, *30*, 5104.
- (31) Boris, D.; Rubinstein, M. *Macromolecules* **1996**, *29*, 7251.
- (32) Naylor, A. M.; Goddard, W. A. *Polym. Prepr.* **1988**, *29*, 215.
- (33) Naylor, A. M.; Goddard, W. A. *J. Am. Chem. Soc.* **1989**, *111*, 2339.
- (34) Chen, Z. Y.; Cui, S.-M. *Macromolecules* **1996**, *29*, 7943.
- (35) Wilfried, C. *J. Chem. Soc., Faraday Trans.* **1996**, *92*, 4151.
- (36) de Gennes, P. G.; Hervet, H. *J. Phys., Lett.* **1983**, *44*, L351.
- (37) Note: according to ISO 31-8, the term "molecular weight" has been replaced by "relative molecular mass", symbol M_r .
- Thus, if this nomenclature and notation were to be followed in this publication, one would write $M_{r,n}$ instead of the historically conventional M_n for the number-average molecular weight, with similar changes for M_w , M_z , and \bar{M}_v , and it would be called the "number-average relative molecular mass". The conventional notation, rather than the ISO notation, has been employed for this publication.
- (38) Grest, G. S.; Fetters, L. J.; Huang, J. S.; Richter, D. *Adv. Chem Phys.* **1996**, *94*, 67.
- (39) Roovers, J. *Macromolecules* **1994**, *27*, 5359.
- (40) Horton, J. C.; Squires, G. L.; Boothroyd, A. T.; Fetters, A. R.; Rennie, A. R.; Glinka, C. J.; Robinson, R. A. *Macromolecules* **1989**, *22*, 681.
- (41) Willner, L.; Jucknischke, O.; Richter, D.; Roovers, J.; Zhou, L.-L.; Toporowski, P. M.; Fetters, L. J.; Huang, J. S.; Lin, M. Y.; Hadjichristidis, N. *Macromolecules* **1994**, *27*, 3821.
- (42) *Small Angle Scattering of X-Rays*; Guinier, A., Fournet, G., Eds.; Wiley: New York, 1955.
- (43) *Small Angle X-Ray Scattering*; Glatter, O., Kratky, O., Eds.; Academic Press: New York, 1982.
- (44) *Polymers and Neutron Scattering*; Higgins, J. S., Benoit, H. C., Eds.; Clarendon Press: Oxford, 1994.
- (45) Burchard, W. *Adv. Polym. Sci.* **1983**, *48*, 1.
- (46) Glatter, O. *Acta Phys. Austriaca* **1977**, *47*, 83.
- (47) Glatter, O. *J. Appl. Crystallogr.* **1977**, *10*, 415.
- (48) Glatter, O. *J. Appl. Crystallogr.* **1980**, *13*, 7, 577.
- (49) Certain commercial materials and equipment are identified in this paper in order to specify adequately the experimental procedure. In no case does such identification imply recommendation by the National Institute of Standards and Technology nor does it imply that the material or equipment identified is necessarily the best available for this purpose.
- (50) Hsaio, B.; Chu, B.; Yeh, F. *NLSLS Newsletter* **1997**, *July*, 1.
- (51) Ziegler, E. *Opt. Eng.* **1995**, *34*, 445.
- (52) Chu, B.; Harney, P. J.; Li, Y.; Linliu, K.; Yeh, F.; Hsaio, B. *Rev. Sci. Instrum.* **1994**, *65*, 597.
- (53) Miyahara, J.; Takahashi, K.; Amemiya, Y.; Kamiya, N.; Satow, Y. *Nucl. Instrum. Methods Phys. Res.* **1986**, *A246*, 572.
- (54) Blanton, T. N.; Huang, T. C.; Toraya, H.; Hubbard, C. R.; Robie, S. B.; Louer, D.; Gobel, H. E.; Will, G.; Gilles, R.; Raftery, T. *Powder Diffraction* **1995**, *10*, 91.
- (55) Megens, M.; van Kats, C. M.; Bosecke, P.; Vos, W. L. *J. Appl. Crystallogr.* **1997**, *30*, 637.
- (56) Mittelbach, P. *Acta Phys. Austriaca* **1964**, *19*, 53.
- (57) Mittelbach, P.; Perod, G. *Kolloid Z. Z. Polym.* **1965**, *202*, 40.
- (58) Burchard, W.; Kajiwara, K.; Nerger, D. *J. Polym. Sci., Polym. Phys. Ed.* **1982**, *20*, 157.
- (59) Pedersen, J. S. *Adv. Colloid Interface Sci.* **1997**, *70*, 171.
- (60) Jackson, C. L.; Chanzy, H. D.; Booy, F. P.; Drake, B. J.; Tomalia, D. A.; Bauer, B. J.; Amis, E. J. *Macromolecules* **1998**, *31*, 6259.
- (61) Mansfield, M. L. *Macromolecules* **1993**, *26*, 3811.
- (62) Personal communication with C. L. Jackson.
- (63) Jansen, J. F. G. A.; de Brabander-van den Berg, E. M. M.; Meijer, E. W. *Science* **1994**, *266*, 1226.
- (64) Gröhn, F.; Bauer, B. J.; Akpalu, Y. A.; Jackson, C. L.; Amis, E. J. *Macromolecules* **2000**, *33*, 6042.

MA0002186